Oil Flow Separation Patterns on an Ogive Forebody

Earl R. Keener*
NASA Ames Research Center, Moffett Field, California

Oil flow patterns on a symmetric tangent ogive forebody having a fineness ratio of 3.5 are presented for angles of attack up to 88 deg at a transitional Reynolds number of 0.8×10^6 (based on base diameter) and a Mach number of 0.25. Results show typical patterns of surface flow separation, the magnitude of surface flow angles, and the extent of laminar and turbulent flow for symmetric, asymmetric, and wake-like flow regimes.

Introduction

BECAUSE the flight envelopes of modern aircraft and missiles include very high angles of attack, an extensive knowledge of the aerodynamics of wing and body combinations over a large range of angles of attack is required. The aerodynamics of bodies at high angles of attack is especially interesting because of the wide variety of flow phenomena that occur at those flight conditions. Several reviews of the development of the current knowledge of body aerodynamics have been presented by Chapman et al.,[1] Nielsen,[2] Spearman,[3] Ericsson and Reding,[4] and Tobak and Peake.[5,6]

Figure 1 (taken from Ref. 7) shows that there are three major boundaries that separate four principal flow regimes that occur[7] over the angle-of-attack range of bodies of 0-90 deg: vortex-free flow at angles up to about 10 deg, symmetric vortex flow at angles of about 10-30 deg, steady asymmetric vortex flow at angles of about 30-60 deg, and unsteady wake-like vortex flow at angles above about 60 deg. The most spectacular flow phenomenon is the occurrence of a large asymmetric flow separation, with a large accompanying side force, when a symmetric body with a pointed nose is pitched to high angles of attack.[7-10] As the angle of attack is increased, the asymmetric flow can occur first on the aft section of the body and move forward with increasing incidence. The largest asymmetric flow and side force are likely to occur when the flow asymmetry reaches the forebody.[8] It was found that a pointed nose with a fineness ratio of 3 or more causes the largest flow asymmetry. It has been suggested that this flow asymmetry is the principal effect of an inviscid instability in the initially symmetric vortex formation and the interaction of the vortices (which increase in strength with incidence) with the surrounding potential flowfield.[10] In addition, the vortex asymmetry is also affected by boundary-layer (viscous) asymmetries caused by transition and separation differences on each side of the body. Asymmetry in either the boundary layer on the windward surface or in the vortex flowfield over the leeward surface will cause asymmetry in the other. It follows that it is important to understand the contribution of each of these hydrodynamically or boundary-layer-induced asymmetries on the total flowfield asymmetry.

The aerodynamic characteristics of forebody models have been investigated to determine the contribution of the forebody to body aerodynamics. Force tests over a large range of Mach numbers, angles of attack, and Reynolds numbers have been reported.[6,8] Side forces were measured that are essentially steady, are as large as 1.5 times the maximum normal force, and vary considerably with Reynolds number. Further, it was found that these side forces can be reduced or eliminated by nose bluntness, nose strakes, nose booms, or the use of forebodies with fineness ratios of 2.5 or less.

In support of the force test program, oil flow visualization tests were made using the forebody models to determine the separation patterns in the various flow regimes. This paper presents oil flow photographs of an ogive forebody fineness ratio (ratio of length ℓ to base diameter d) of 3.5 at angles of attack of 0-90 deg, at a Mach number of 0.25, and at a Reynolds number of 0.8×10^6 (referenced to base diameter). At this Reynolds number and at high angles of attack, there is a large side force and a transitional (laminar/turbulent) boundary layer. The photographs give an indication of typical patterns of surface flow separation, the magnitude of surface flow angles, and the extent of laminar and turbulent flow for the symmetric, asymmetric, and wake-like flow separation regimes.

Experiment

Steady and unsteady forces and oil flow and sublimation flow visualization results were obtained in the 12 ft pressure wind tunnel at Ames Research Center at $M=0.25$, $R_d=0.8\times10^6$, and $\alpha=0$-90 deg. The strain gage balance forces were recorded on an oscillograph to determine the occurrence and degree of unsteadiness. The turbulence velocity level has been measured to be less than 0.3% of the freestream velocity. Schlieren results were obtained in the 6×6 ft transonic wind tunnel (Ames Research Center) at $M=0.25$.

The model was an ogive forebody with a fineness ratio (ℓ/d) of 3.5 and was one of six forebody models that were tested in the investigation of forebody characteristics.[7,8] A cylindrical afterbody ($\ell/d=3.5$), which could be clamped to the sting but be free of the forebody, was used in some of the tests, from which it was determined that base effects did not change the basic flow and force characteristics over the forebody.

For these oil flow tests, the bare models were coated uniformly with a mixture of lampblack (for color) and motor oil of various viscosities (depending on the velocity and incidence); a few drops of oleic acid were added to the oil to insure better dispersion of the lampblack in the oil.[11] The local aerodynamic flow forces this oil mixture into streaks that migrate in the direction of flow (skin friction lines). The sublimation technique[11] was used to determine the position of boundary-layer transition. The models were sprayed with a saturated solution of biphenyl dissolved in trichloroethane, which is less flammable than the commonly used petroleum ether. This solution, which dries on contact with the model surface, presents a white appearance. As the wind tunnel is operated, the biphenal coating sublimes faster in regions of turbulent flow than in the regions of laminar flow. Usually, a line of demarcation can be seen between these two regions. The schlieren photographs were obtained in the 6×6 ft tunnel at $M=0.25$, using a standard mercury vapor lamp schlieren

Received Nov. 12, 1981; revision received Aug. 17, 1982. This paper is declared a work of the U. S. Government and therefore is in the public domain.

*Research Scientist. Associate Fellow AIAA.

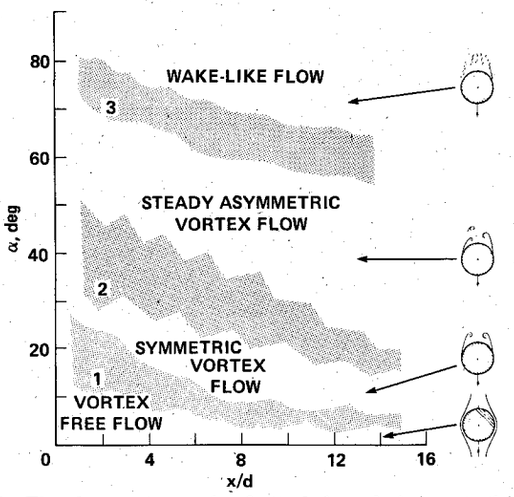

Fig. 1 The three onset angle-of-attack boundaries separating the four major types of cross-sectional aerodynamic flow patterns for pointed bodies.

system. The centers of the vortex cores were seen as abrupt changes in light intensity from dark to light.

Effect of Angle of Attack on Oil Flow Patterns

The oil flow patterns were thoroughly documented for the ogive forebody ($\ell/d=3.5$) at $R_d=0.8\times10^6$. This Reynolds number is beyond the upper limit of the critical number range ($0.1\text{-}0.5\times10^6$) for a circular cylinder; as a result, the effects of boundary-layer transition are likely to occur. Photographs were taken at 5 deg increments in the angle of attack to insure that flow patterns would be obtained in each of the vortex flow regimes. Representative photographs are shown in Fig. 2 for angles of attack of 5, 10, 20, 30, 40, 55, 70, and 88 deg. Also shown are sublimation photographs at $\alpha=20$ and 40 deg. Figure 3 presents sketches of the oil flow patterns on the body surface as if it were "unwrapped." They show two principal features of the surface flow topology: mean skin friction lines and separation lines. A key to the labels on the sketches is given in Fig. 3. [The reader might wish to read first the discussion of the results for $\alpha=40$ deg (Figs. 2e and 3e) at which most of the basic flow patterns discussed herein appear.]

It should be noted that oil flow patterns can be easily misinterpreted. Moreover, it is difficult to construct the correct external flowfield from the surface flow patterns. Sometimes, there is more than one possible pattern. The interpretations given herein are, of course, those of the author; however, they have been discussed with the other investigators listed in the acknowledgments, and the author has tried to incorporate their suggestions and to reconcile differences in interpretation.

Angle of Attack: 5 deg

Two oil flow photographs are shown in Fig. 2a for the left side at body meridian angles of $\theta=135$ and 180 deg; sketches of the flow pattern are presented in Fig. 3 for the "unwrapped" surface. First, there is a noticeable crossflow caused by incidence. The angle δ_s that the local oil flow streaks make with the freestream flow direction was measured along the sides at $\theta=\pm90$ deg. Near the nose at $x/\ell=0.2$ (where x is the axial length from the nose tip and ℓ is the forebody length), $\delta_s\approx24$ deg, which is about 2.5 times the external potential angle at the edge of the boundary layer of $\delta_e=2\alpha=10$ deg. [δ_e is determined by calculating the crossflow component of velocity (normal to the axis and parallel to the surface) at $\theta=90$ deg for a cylinder that, from potential theory, is twice the crossflow component of the freestream velocity V_N. This velocity of $2V_N$ is then combined with the axial component of the freestream velocity, $V_\infty\cos\alpha$. The resulting flow angle is $\delta_e=2\tan\alpha$.] Rearward of $x/\ell=0.2$, the surface flow angle decreases with increasing length until $\delta_s\approx\delta_e=10$ deg at $x/\ell\approx0.5$ and beyond to the base. The significantly higher oil flow angles ahead of $x/\ell=0.5$ mean that the local velocity distribution in the boundary layer between the edge and the surface is highly skewed in the direction ahead of the inviscid streamline.

In the forward part of the forebody, the oil thickens for a short distance, forming a patch (probably the accumulation of oil caused by a thickening laminar boundary layer). However, note that within the patch of oil there are regularly spaced heavy oil streaks that are at an angle to the local skin friction lines. The cause of these oil streaks is not known; however, the oil flow pattern was expected to be smooth at $\alpha=5$ deg. Such transitional regions as this are often locally unsteady (intermittent). Downstream of the thickened patch of oil, the oil is scrubbed (thinned), indicating that the flow is turbulent to the base. On the sides near the base it is suspected that boundary-layer transition occurs along an oblique line that starts at the patch of oil (Fig. 3a), because similar transition was found at $\alpha=20$ deg. On the leeward surface near the base there is no indication of reversal of the crossflow (normal) component of the direction of flow; that is, there is no crossflow separation near the base.

Angle of Attack: 10 deg

The oil streak angles δ_s on the sides at $\theta=\pm90$ deg are above 41 deg at $x/\ell=0.2$ (Fig. 2b). This is about twice the potential angle of 2α; consequently, the boundary-layer flow continues to be highly skewed over the forward part. The patch of thickened oil that occurred at $\alpha=3$ deg develops into a band of oil on each side at $\alpha=10$ deg, located at $\theta=\pm135$ deg and extending from the nose tip to $x/\ell=0.45$, where the ends of the oil bands appear to be swept away by the crossflow behind them. It is believed that local primary laminar separation (LS) occurs at the band of oil at $0<x/\ell<0.45$. The symmetric separation lines on each side exist to the nose tip; however, according to conical flow concepts, local separation at the nose tip was not expected until $\alpha=\delta_N=16.5$ deg, where δ_N is the nose semiapex angle of 16.5 deg for the $\ell/d=3.5$ ogive.

It is interesting that in the region away from the nose at $0.2<x/\ell<0.45$ the boundary layer appears to reattach (R) leeward of the band of oil, because the oil streaks can be seen to continue toward the leeward. There is considerable disagreement concerning the details of the flowfield at the nose, because the oil flow lines are not entirely clear in such a small region. The effective Reynolds number is low in this region, so that the flow should normally be completely separated into a pair of separation vortices, with reattachment at $\theta=180$ deg. However, consider also that there is a strong axial flow on the lee side of the nose because the local angle is positive ($\delta_N-\alpha=6.5$ deg). This strong axial flow facilitates reattachment of the separated flow on the leeward surface at $\theta<180$ deg. Reattachment can be seen farther rearward at $0.2<x/\ell<0.45$; however, at $x/\ell<0.2$, the oil flow streaks are not entirely clear in Fig. 2. It is the author's opinion that the original photographs indicate that the leeward flow is axially directed all the way to the nose, so that the strong axial flow reattaches the laminar separated flow all the way forward to the nose. This flow pattern does not really violate the impulsive analogy of Allen and Perkins[12] which many use as a guide to cross-sectional flowfields. (Allen and Perkins noted that the cross-sectional flowfields which develop with length over long bodies at high angles of attack are similar to the flowfields which develop with time for a two-dimensional circular cylinder impulsively started from rest.) Thus, one might expect to first see attached flow at the nose followed by the development of a symmetrical pair of vortices and,

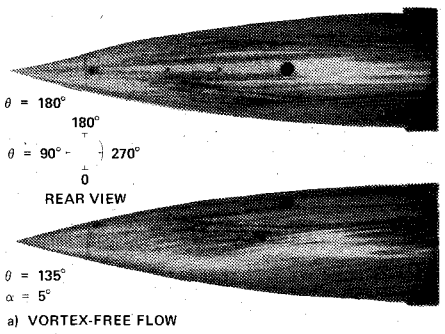

a) VORTEX-FREE FLOW

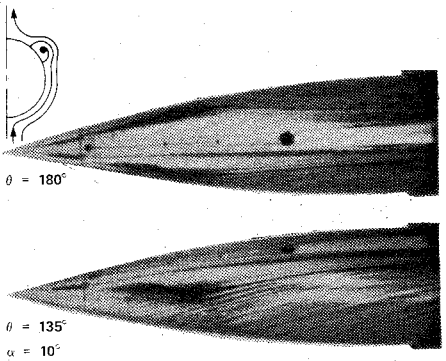

b) LAMINAR SEPARATION

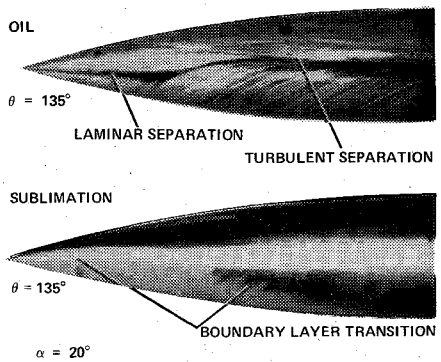

α = 20°

c) SYMMETRIC VORTEX FLOW

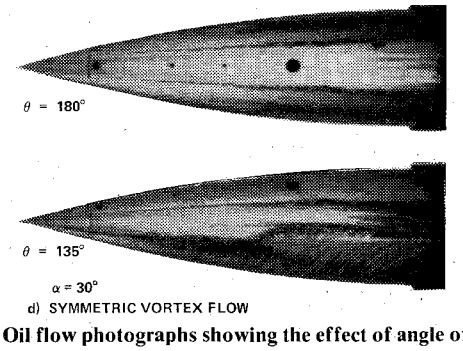

α = 30°

d) SYMMETRIC VORTEX FLOW

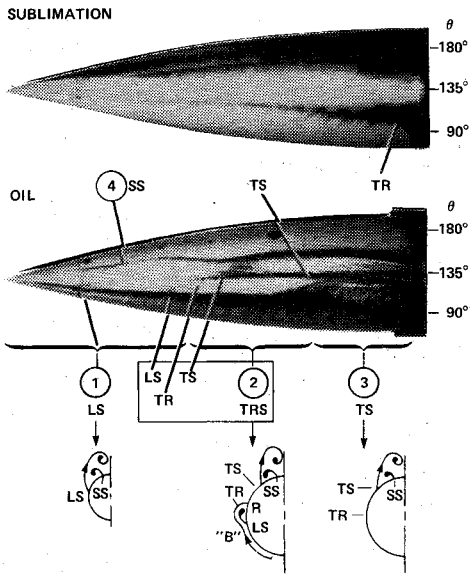

PRINCIPAL FEATURES:

1. PRIMARY LAMINAR SEPARATION, LS
2. PRIMARY TRANSITIONAL SEPARATION, TRS = (LS + TR + R + TS)
3. PRIMARY TURBULENT SEPARATION, TS
4. SECONDARY SEPARATION, SS

α = 40°, C_Y = 0.5

e) SLIGHTLY ASYMMETRIC VORTEX FLOW

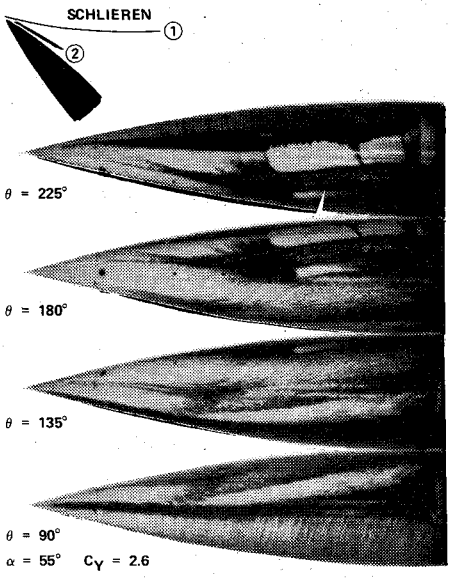

α = 55° C_Y = 2.6

f) ASYMMETRIC VORTEX FLOW

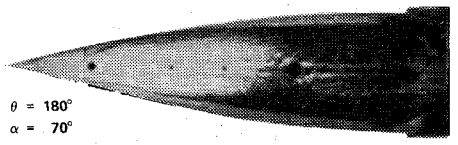

g) PARTIAL WAKE-LIKE FLOW

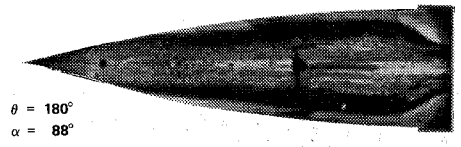

h) UNSTEADY WAKE-LIKE VORTEX FLOW

Fig. 2 Oil flow photographs showing the effect of angle of attack at a transitional Reynolds number of $R_d = 0.8 \times 10^6$, $M = 0.25$, $\ell/d = 3.5$ ogive.

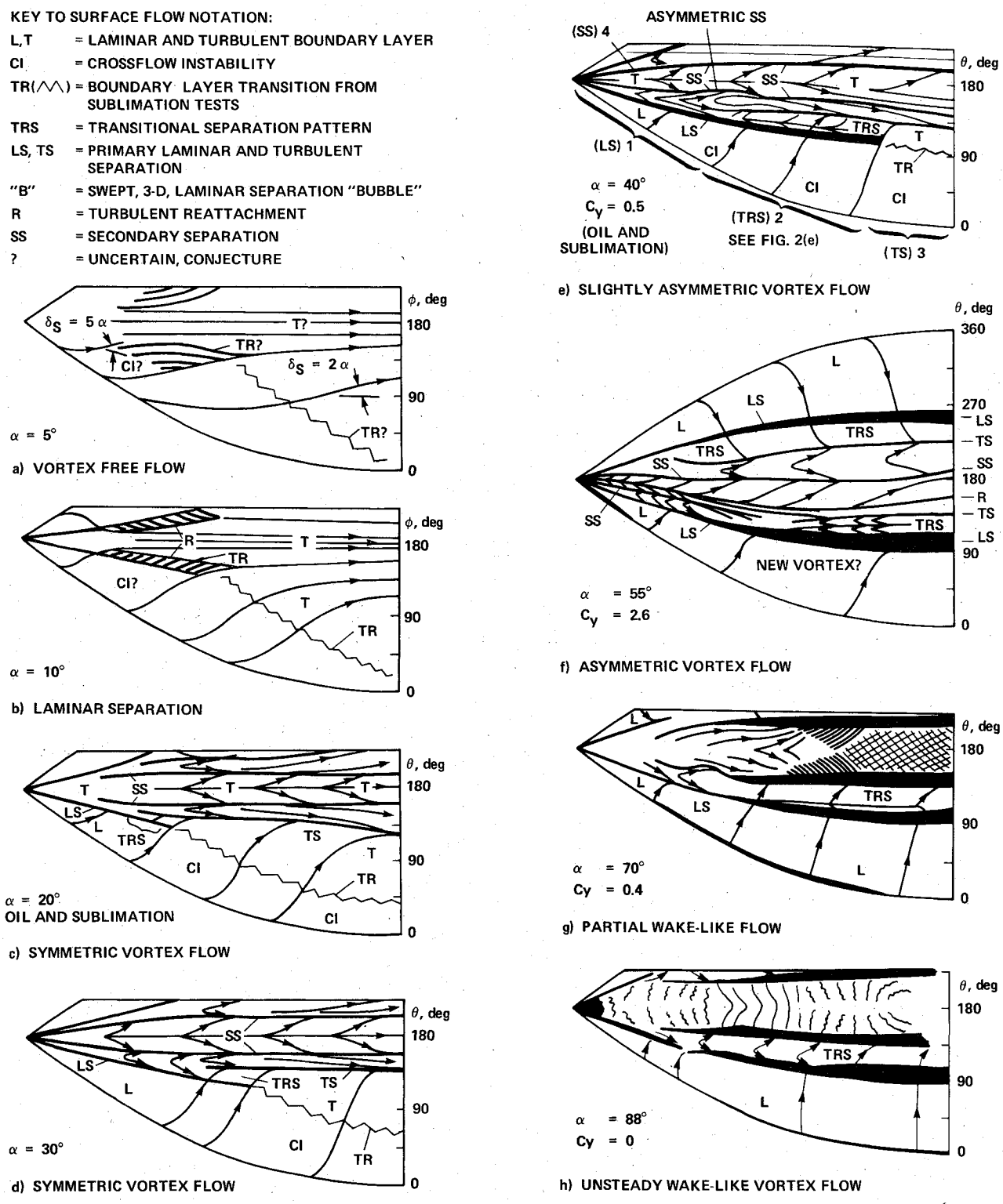

Fig. 3 Sketches of oil flow patterns (Fig. 2) showing the effect of angle of attack at a transitional Reynolds number of $R_d = 0.8 \times 10^6$, $M = 0.25$, $\ell/d = 3.5$ ogive.

finally, farther downstream on a long body by asymmetric alternating vortex shedding. The attached flow does not occur at the nose at $\alpha = 10$ deg, but the flow separates immediately as a result of the elevated Reynolds number. The separated flow reattaches (in the author's opinion) because of the axial flow, which is not part of the impulsive flow analogy.

Note also that the laminar separation is interrupted on the left side by a disturbance at the junction of the nose tip. One can expect that this type of flow disturbance is highly intermittent, locally wiping out the separation line.

Rearward of $x/\ell = 0.45$ the band of oil does not exist and the oil is scrubbed, indicating that boundary-layer transition (TR) occurs on the sides and terminates the laminar separation. The weak laminar separation vortex must be swept away in the crossflow. The oil streaks on the lee side near the base converge slightly, indicating that turbulent separation is imminent in this region.

Angle of Attack: 20 deg

Both an oil flow and sublimation photograph are shown (Fig. 2c; also refer to the sketches in Fig. 3c) for the left side at $\theta = 135$ deg. The principal features in the oil flow patterns are three types of primary separation. First, there is *primary laminar separation* (LS) at a meridian angle of $\theta \approx \pm 115$ deg,

starting at the nose tip and ending at $x/\ell \approx 0.35$. The line of accumulated oil is a continuation of the successive stages of development of the oil pattern near the nose that led to the patch of oil at $\alpha = 5$ deg and the band of oil at $\alpha = 10$ deg. However, near the nose the details of the flow are again obscure on the leeward surface; for example, the reversed flow lines and reattachment line are not clearly seen.

The second type of primary separation occurs in a small but very interesting region at $0.2 < x/\ell < 0.35$ where two primary separation lines occur. This region is called herein *primary transitional separation* (TRS). It is much more prominent at $\alpha = 40$ deg and is discussed more fully in the $\alpha = 40$ deg subsection.

The third type of primary separation is *primary turbulent separation* (TS) which occurs at $\theta \approx \pm 140$ deg, in the region rearward of $x/\ell \approx 0.35$ where the end of the primary laminar separation line occurs. In this region, boundary-layer transition occurs upstream (windward) of the laminar separation lines on the sides and, as a result, the laminar separation is changed to turbulent separation. This effect of boundary-layer transition is verified in the sublimation photograph in Fig. 2c. Note that the white sublimation material ends where the oil separation line ends at $x/\ell \approx 0.35$, indicating that transition occurs at this location. Rearward of $x/\ell \approx 0.35$, where the oil line disappears, the sublimation material ends along a ragged path of decreasing meridian angle to the windward, indicating the location of transition.

Barely noticeable in the sublimation photographs (but easily seen on the model during the test) are striations in the sublimation material that can be seen from the base to the nose throughout the region of the highly skewed boundary layer. The striations are oriented roughly along the same direction as the oil streaks; they indicate the presence of vortices that are produced in the boundary layer by *crossflow inflection instability*, similar to that which occurs on swept wings.[13] The occurrence of these vortices on wings is dependent on Reynolds number and angle of sweep. On bodies at high Reynolds numbers the conditions exist for the appearance of these vortices over the entire body length as soon as the body departs from zero incidence. The presence of these vortices on swept wings is known to induce early transition to a turbulent boundary layer; however, they do not necessarily affect boundary-layer separation.

Finally, at $\theta \approx \pm 160$ deg, a *secondary separation line* (SS) occurs which can be traced forward ahead of the nosepiece junction but not to the tip. Secondary separation results from the separation of the reversed leeward crossflow streaming from the line of reattachment of the primary vortex flow at $\theta = 180$ deg. The resulting secondary vortex rotates in a direction opposite to that of the primary vortex.

Angle of Attack: 30 deg

Primary laminar separation (LS) lines are clearly identified by reverse crossflow in the leeward oil flow streaks (Figs. 2d and 3d). They extend from the nose tip to $x/\ell = 0.60$ and are located at $\theta \approx \pm 110$ deg. The region for the simultaneous occurrence of two primary separation lines (TRS) moves slightly rearward to $0.4 < x/\ell < 0.65$ at $\alpha = 30$ deg. (See the following subsection on $\alpha = 40$ deg for a description of this flow pattern.) Primary TS occurs over the rearward 40% length at $\theta \approx 140$ deg. SS occurs at $\theta \approx \pm 160$ deg over the full length of the forebody.

Angle of Attack: 40 deg

At this test condition, four of the five principal types of flow separation that were found in the study are very prominent and are labeled in the oil flow photograph shown for $\theta = 135$ deg (Fig. 2e). Also shown is a sublimation photograph for $\theta = 135$ deg showing the location of boundary-layer transition. Three types of primary separation patterns occur: 1) laminar, 2) "transitional," and 3) turbulent. These patterns appear at the lower angles, but the transitional pattern is not as prominent as at $\alpha = 40$ deg. Secondary separation is the fourth principal separation pattern seen at $\alpha = 40$ deg.

Primary laminar separation (LS) (Figs. 2e and 3e) is indicated by the oil line that occurs at $\theta \approx \pm 100$ deg. Region 1 (regions are designated by circled numbers in Fig. 2e) for primary laminar separation is shown to occur from the tip back to $x/\ell \approx 0.3$. However, note that the laminar separation line extends to $x/\ell \approx 0.8$ and that the region of $0.3 < x/\ell < 0.8$ is labeled 2. In this region *two primary separation lines* occur. This same flow pattern was noted at $\alpha = 20$ and 30 deg for small regions; however, at $\alpha = 40$ deg this flow pattern is prominent and extensive. Region 2 has been herein termed *primary transitional separation* (TRS) and it consists of primary laminar separation, followed by boundary-layer transition and reattachment, and finally primary turbulent separation. "Transitional" is intended to mean that this pattern is transitional between the primary laminar and primary turbulent separation patterns. Although this pattern is not as well known in two-dimensional cylinder flows, Jones et al.[14] show an oil flow pattern at $R_d = 1.6 \times 10^6$, similar to that of region 2, having two primary separations—laminar and turbulent. This separation pattern is the next natural hierarchy of flow separation, occurring as the Reynolds number is increased after laminar separation. It occurs when the local Reynolds number is high enough that transition occurs in a short distance following laminar separation.

In the pattern of primary transitional separation, note that the initial primary laminar separation and the quick reattachment of the flow encloses the cross-sectional flow in a "bubble-like" flow pattern (Fig. 2e). The term *laminar separation bubble* has been used informally in the description of two-dimensional laminar separation that is followed by transition in the shear layer shortly after separation, so that the shear layer bends toward the surface and reattaches on the surface, forming an enclosed bubble. A similar oil separation line has been observed on the leading edges of swept wings; these have also been informally called laminar separation bubbles because the flow reattaches in a short distance, forming a short bubble-like separation region. However, there is a fundamental difference in the flow within the bubble between two- and three-dimensional flows. In two-dimensional separation, the flow model is a closed circulation and the streamlines within the bubble form closed paths. In three-dimensional separated flow there must be transverse flow parallel to the separation line. As a result of this flow, viewed in a crossflow plane (cf. sketch in Fig. 2e), the circulation zone is not closed and the projections of streamlines in this plane do not form closed paths. Instead, the bubble has the form of a growing vortex. In this paper, the informal term "swept bubble" (B) is used to refer to this type of laminar flow separation. Note that all bubbles are initiated by primary laminar separation (LS), with the term primary referring to the fact that in the crossflow plane, the separation is being fed from boundary-layer fluid originating at the windward meridian (in contrast to secondary separation).

In this regard it is interesting to note that the primary laminar separation that occurs at $\alpha = 10$ deg near the nose might also be called a swept bubble wherever reattachment occurs shortly after separation ($\theta < 180$ deg).

Primary turbulent separation (TS), region 3 in Figs. 2e and 3e, occurs when transition moves upstream (toward $\theta = 0$) as a result of the higher local Reynolds number for the larger diameter of the rear section, eliminating the primary laminar separation and the swept bubble. Consequently, the turbulent flow remains attached until $\theta \approx 140$ deg, where primary turbulent separation occurs. The sublimation photograph verifies that transition occurs along the lee of the swept bubble and moves upstream at the rear of the forebody. The small swept bubble appears to be swept away into the boundary-layer crossflow at the end of the oil separation line.

Also, striations were seen in the sublimation material from the base forward to $x/\ell \approx 0.2$, which indicate the presence of vortices from crossflow inflectional instability. Note that in region 3, TS is prominent for $\alpha = 30$ deg, but is greatly reduced at $\alpha = 40$ deg by the increasing length of transitional separation. This verifies that the effective Reynolds number for the boundary layer is lower for $\alpha = 40$ deg than for $\alpha = 30$ deg (as discussed in Ref. 3), because the effective boundary-layer length of run is lower for $\alpha = 40$ deg than for $\alpha = 30$ deg.

The last feature in Fig. 2e is the SS line 4 that occurs on the lee of the primary separation line at $\theta \approx \pm 160$ deg and extends to the nose tip. In this type of flow pattern, the flow from the primary flowfield circulates to the lee surface around the primary separation vortex, reattaches at $\theta = 180$ deg, and moves toward $\theta = 160$ deg where it separates again into a vortex filament that circulates in the opposite direction to the primary vortex.

Finally, the first small *flow asymmetry* appears in the leeward oil flow pattern in the secondary separation line (see sketch in Fig. 3e). As a result, a small measured side force occurs ($C_Y = 0.5$).

Angle of Attack: 55 deg

All of the features of the oil flow pattern are asymmetric and a large, relatively steady asymmetric force of $C_Y = 2.6$ (Figs. 2f and 3f) was measured. Although the flow has some unsteadiness, the unsteadiness does not predominate. Note that vortex traces are shown as sketched from schlieren photographs. These vortices are highly asymmetric and slightly unsteady but do not switch position. The first vortex is shed near the nose tip and passes high above the forebody almost straight back from the nose tip. The second vortex is located close to the surface and disappears at midlength.

The LS lines extend the full length on both sides but are asymmetrically located at $\theta \approx -100$ deg ($+260$ deg) on the right side and $\theta \approx 80$ deg on the left, which is correct for a right-side force. TRS is clearly indicated on the right side, starting at $x/\ell \approx 0.2$, by the overlapping primary laminar separation and turbulent separation lines. On the left side, the turbulent separation line extends ahead to $x/\ell \approx 0.4$, compared with its extension to about 0.2 on the right, so that the transitional separation is asymmetrically disposed longitudinally as well as circumferentially. In addition, the SS lines on the lee are very asymmetric. The right separation line extends at least to the midlength, where it is close to the top centerline. Consequently, the oil flow lines from the right-hand vortex cross over the lee centerline to the left and disappear at $x/\ell \approx 0.5$. The left secondary separation line is pushed to the left side to $\theta \approx 140$ deg. This oil line seems to branch into several lines at $x/\ell \approx 0.3$, which might indicate the location where the first vortex is finally shed (detached from the surface). Sometimes it is stated that a vortex sheet "tears" when it is shed; however, from topological considerations,[5] vortices cannot "tear" but rather the sheet must be continuous. There has to be a continuity to the vortex structure and the accompanying separation lines. In addition, a new vortex must form on the left side where the first vortex is shed; however, this is also not clear in the oil flow pattern. Consequently, it is felt that the topology of these patterns at $\alpha = 55$ deg is still not fully understood.

Sublimation photographs (not shown) show striations on the windward surface from the base forward to near the nose, indicating that crossflow inflectional instability also occurs at this angle.

Angle of Attack: 70 deg

The oil flow pattern exhibits a small asymmetry on the lee, which is considerably reduced from that at $\alpha = 55$ deg; however, the laminar separation on each side is symmetric (Figs. 2g and 3g). A prominent difference from the pattern at $\alpha = 55$ deg occurs on the leeward surface over the rear half, where the oil accumulates into a large dark patch with no flow lines. From this flow pattern and from those at $\alpha = 80$ and 88 deg, it is certain that in the region of the rear half the flow separates into an unsteady wake-like flow similar to that behind a swept circular cylinder. In such a flow the vortices leave the surface on each side in an alternating pattern that could be either periodic (like a vortex street) or random, depending on the Reynolds number.

Angle of Attack: 88 deg

The accumulated patch of oil on the lee indicates wake-like separation extending forward to the nose tip (Figs. 2h and 3h). The side force is zero for this angle. Note that the flow separation on the sides is transitional forward to $x/\ell \approx 0.2$. Jones[14] showed transitional flow on a circular cylinder transverse to the flow at $R_d = 1 \times 10^6$.

Measured Surface Flow Angles

Figure 4 presents the measured surface oil streak angles (skin friction line angles) at $\theta = \pm 90$ deg on the sides of the $\ell/d = 3.5$ ogive and of the 20 deg cone. Data for the 20 deg cone at $\alpha = 36$ deg are also included for comparison. As mentioned previously in the discussion of the oil flow patterns, the angles near the nose at $\alpha = 5$ and 10 deg are about 5α, which is more than twice the potential flow angle of 2α at low angles of attack; this indicates that the boundary-layer velocity profiles are highly skewed near the nose. Further, it is interesting that with increasing angle of attack, the flow angle δ_s follows close to the curve for $\tan^{-1}(5\tan\alpha)$. Rearward of the nose, the flow angle decreases with increasing distance from the nose until, over the rear half of the forebody, the oil flow angles are close to the potential flow angle of $\tan^{-1}(2\tan\alpha)$. Between $\alpha = 40$ and 70 deg the flow angles on each side are asymmetric because of the asymmetry in the vortex flowfield (see shaded region in Fig. 4). Note that most of the curves have inflections near $\alpha = 20$ and 40 deg. These angles are close to the onset of symmetric and asymmetric vortex flow, respectively, and these inflections represent a retardation in rate of change in surface flow angle with incidence. Evidently, the favorable crossflow pressure gradient is responsible for the increase in flow angle with increasing incidence and the resulting skewing of the boundary-layer velocity profiles. Therefore, the inflections in the δ_s vs α curves must result from changes in the variation of the crossflow pressure gradient with incidence, caused by the onset of the formation of the symmetric vortex flowfield and, at higher incidence, by the onset of vortex asymmetry.

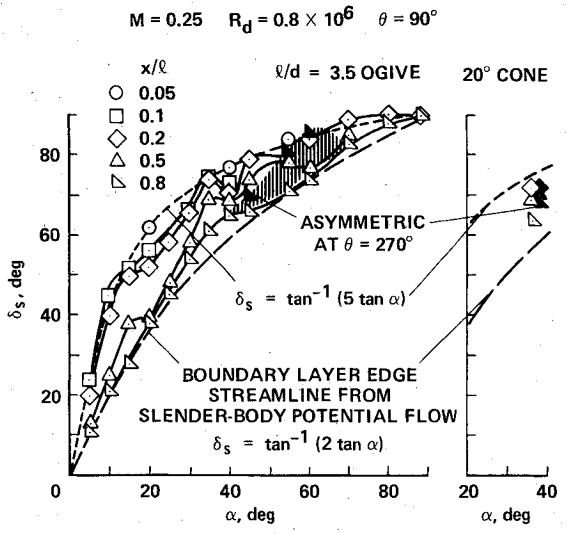

Fig. 4 Surface oil flow (skin friction line) angles on the sides of two forebody models; $R_d = 0.8 \times 10^6$, $M = 0.25$, $\theta = \pm 90$ deg.

The data for the 20 deg cone at $\alpha = 36$ deg (Fig. 4) show a smaller variation with cone length than for the ogive forebody; hence, the flow is more conical than for the ogive with respect to the surface flow angles. The measured angle for the cone is about 70 deg at $x/\ell \geq 0.2$, which lies between the potential flow angle of about 56 deg and the skewed flow angle of about 73 deg that occurs on the nose of the ogive. Therefore, the cone surface flow angles are greatly skewed from the potential over most of the cone length. The highly skewed boundary layer has the potential of inducing inflectional instability in the velocity profiles and promoting transition. The occurrence of inflectional instability was verified by sublimation tests at $\alpha = 20$, 40, and 55 deg in which striations appeared on the windward surface in the sublimation materials. Note that the difference in surface flow angles between the cone and the ogive indicates that the shape of the forebody can affect the local boundary-layer flow conditions through the distribution of crossflow velocity profiles.

Conclusion

Oil flow, sublimation, and schlieren flow visualization tests about ogival ($\ell/d = 3.5$) and conical forebodies were conducted at a Mach number of 0.25 over an angle of attack range of 0-90 deg.

The Reynolds number of 0.8×10^6 was selected because an interesting mixture of laminar and turbulent boundary-layer flow patterns exist at this number, and there is a large side force at high incidence. The oil flow photographs show the surface flow patterns that exist in the four principal flow regimes: 1) unseparated, potential, vortex-free flow; 2) symmetric vortex flow; 3) asymmetric vortex flow; and 4) wake-like, unsteady vortex flow. Symmetric vortex flow can be detected between angles of attack of 10 and 20 deg, starting at the nose. Asymmetric vortex flow is first seen over the rear half at $\alpha = 40$ deg.

Three types of primary separation patterns were found along the length of the forebody because of the influence of boundary-layer transition: 1) primary laminar separation, which occurs near the nose; 2) primary transitional separation, which occurs near the midsection (this type of separation pattern consists of a combination of laminar separation, turbulent reattachment, and turbulent separation); and 3) primary turbulent separation, which occurs over the remainder of the forebody. The extent of these three types of primary separation depends on the angle of attack.

Another interesting effect is the large surface flow angles near the nose tip. At low incidence these angles are more than twice the potential flow angle of 2α at the edge of the boundary layer on each side. These large angles result in large skewing of the boundary-layer velocity profiles, which has the potential of inducing inflectional instability and promoting transition. The occurrence of crossflow inflectional instability was verified at angles of attack of 20, 40, and 55 deg by sublimation tests in which striations were observed to result from the presence of the array of vortices that are produced by the instability.

Acknowledgments

The author thanks Dr. Gary Chapman and Mr. Murray Tobak, Ames Research Center, and Dr. Mark Morkovin, recently retired Professor, Mechanical and Aerospace Engineering Dept., Illinois Institute of Technology, for important contributions to the analysis of the flow visualization results.

References

[1] Chapman, G. T., Keener, E. R., and Malcolm, G. N., "Asymmetric Aerodynamic Forces on Aircraft Forebodies at High Angles of Attack—Some Design Guides," *Stall-Spin Problems of Military Aircraft,* AGARD-CP-99, Nov. 1976.

[2] Nielsen, J. N., "Nonlinearities in Missile Aerodynamics," AIAA Paper 78-20, Jan. 1978.

[3] Spearman, M. L., "Historical Development of Worldwide Guided Missiles," AIAA Paper 78-210, Jan. 1978.

[4] Ericsson, L. E. and Reding, J. P., "Vortex-Induced Asymmetric Loads in 2-D and 3-D Flows," *Journal of Spacecraft and Rockets,* Vol. 18, March-April 1981, p. 97.

[5] Tobak, M. and Peake, D. J., "Topology of Two-Dimensional and Three-Dimensional Separated Flows," AIAA Paper 79-1480, July 1979.

[6] Tobak, M. and Peake, D. J., "Topology of Three-Dimensional Separated Flows," NASA TM-81294, 1981.

[7] Keener, E. R., Chapman, G. T., and Kruse, R. L., "Effects of Mach Number and Afterbody Length of Onset of Asymmetric Forces on Bodies at Zero Sideslip and High Angles of Attack," AIAA Paper 76-66, Jan. 1976.

[8] Kruse, R. L., Keener, E. R., Chapman, G. T., and Claser, G., "Investigation of the Asymmetric Aerodynamic Characteristics of Cylindrical Bodies of Revolution with Variations in Nose Geometry and Rotational Orientation at Angles of Attack to 58° and Mach Numbers to 2," NASA TM-78533, 1979.

[9] Keener, E. R. and Chapman, G. T., "Onset of Aerodynamic Side Forces at Zero Sideslip on Symmetric Forebodies at High Angles of Attack," AIAA Paper 74-770, 1974.

[10] Keener, E. R. and Chapman, G. T., "Similarity in Vortex Asymmetries over Slender Bodies and Wings," *AIAA Journal,* Vol. 15, Sept. 1977, pp. 1370-1372.

[11] Maltby, R. L., "Flow Visualization in Wind Tunnels Using Indicators," AGARDograph 70, April 1962.

[12] Allen, H. J. and Perkins, E. W., "Characteristics of Flow Over Inclined Bodies of Revolution," NACA RM-A50L07, 1951.

[13] Chapman, G. T., "Some Effects of Leading-Edge Sweep on Boundary-Layer Transition at Supersonic Speeds," NASA TN D-1705, 1961.

[14] Jones, G. W. Jr., Cincotta, J. J., and Walker, R. W., "Aerodynamic Forces on a Stationary and Oscillatory Circular Cylinder at High Reynolds Numbers," NASA TR R-300, 1979.